

Multifunctional succinate additive for flexible perovskite solar cells with more than 23% power-conversion efficiency

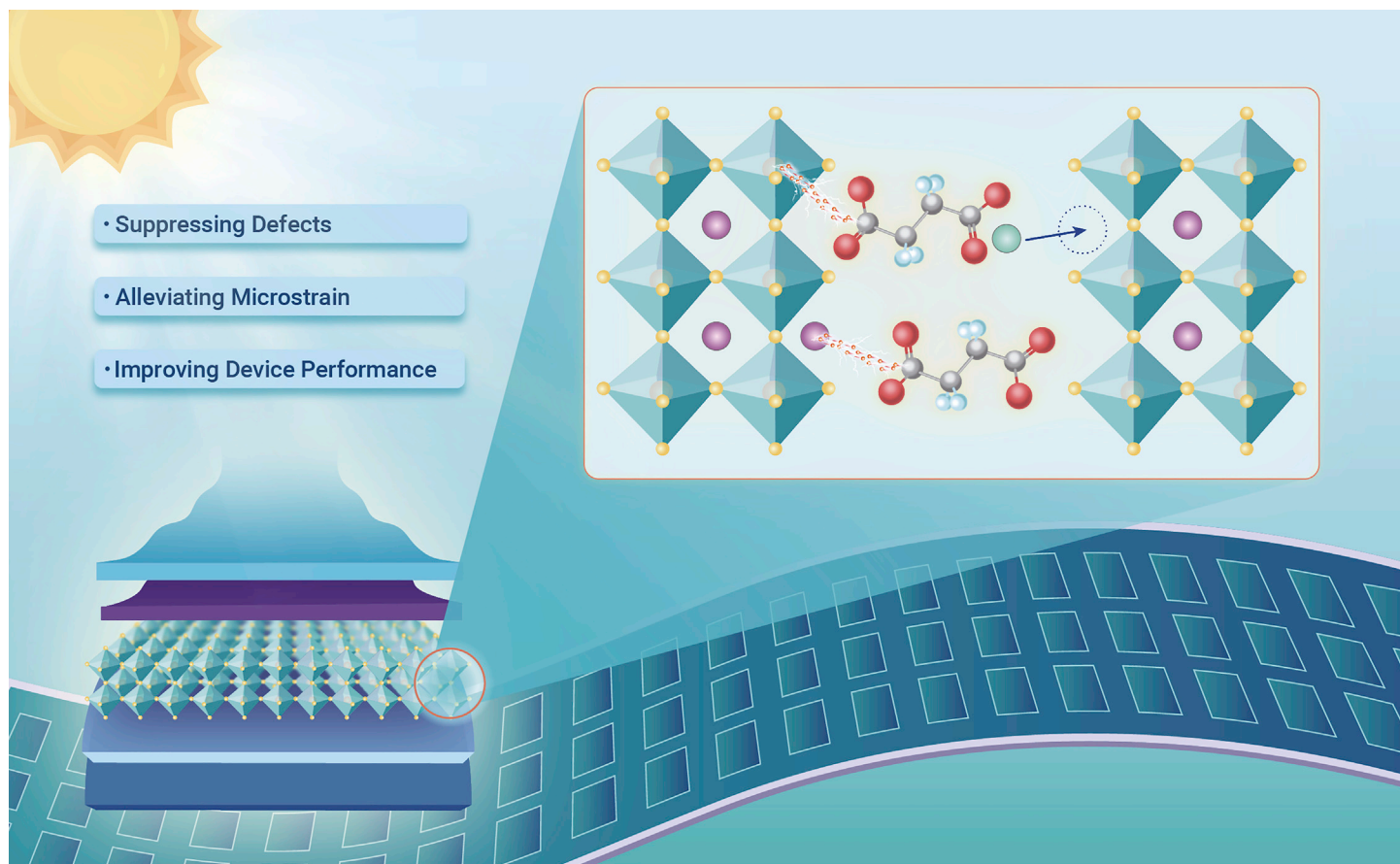
Minghao Li,¹ Junjie Zhou,¹ Liguo Tan,¹ Hang Li,¹ Yue Liu,¹ Chaofan Jiang,¹ Yiran Ye,¹ Liming Ding,² Wolfgang Tress,³ and Chenyi Yi^{1,*}

*Correspondence: yicy@tsinghua.edu.cn

Received: June 9, 2022; Accepted: August 31, 2022; Published Online: September 6, 2022; <https://doi.org/10.1016/j.xinn.2022.100310>

© 2022 The Author(s). This is an open access article under the CC BY-NC-ND license (<http://creativecommons.org/licenses/by-nc-nd/4.0/>).

GRAPHICAL ABSTRACT



PUBLIC SUMMARY

- FPSCs hold promise as power sources for flexible electronics and spacecraft
- Succinate additives enable high-quality perovskite films with reduced microstrain
- An efficiency of 25.4% has been achieved for perovskite solar cells
- An efficiency of 23.6% has been achieved for FPSCs with excellent durability



Multifunctional succinate additive for flexible perovskite solar cells with more than 23% power-conversion efficiency

Minghao Li,¹ Junjie Zhou,¹ Liguo Tan,¹ Hang Li,¹ Yue Liu,¹ Chaofan Jiang,¹ Yiran Ye,¹ Liming Ding,² Wolfgang Tress,³ and Chenyi Yi^{1,*}

¹State Key Laboratory of Power System, Department of Electrical Engineering, Tsinghua University, Beijing 100084, China

²Center for Excellence in Nanoscience (CAS), Key Laboratory of Nanosystem and Hierarchical Fabrication (CAS), National Center for Nanoscience and Technology, Beijing 100190, China

³Institute of Computational Physics (ICP), ZHAW School of Engineering, Wildbachstr. 21, Winterthur 8400, Switzerland

*Correspondence: yicy@tsinghua.edu.cn

Received: June 9, 2022; Accepted: August 31, 2022; Published Online: September 6, 2022; <https://doi.org/10.1016/j.xinn.2022.100310>

© 2022 The Author(s). This is an open access article under the CC BY-NC-ND license (<http://creativecommons.org/licenses/by-nc-nd/4.0/>).

Citation: Li M., Zhou J., Tan L., et al., (2022). Multifunctional succinate additive for flexible perovskite solar cells with more than 23% power-conversion efficiency. *The Innovation* 3(6), 100310.

Flexible perovskite solar cells (FPSCs) have emerged as power sources in versatile applications owing to their high-efficiency characteristics, excellent flexibility, and relatively low cost. Nevertheless, undesired strain in perovskite films greatly impacts the power-conversion efficiency (PCE) and stability of PSCs, particularly in FPSCs. Herein, a novel multifunctional organic salt, methylammonium succinate, which can alleviate strain and reinforce grain boundaries, was incorporated into the perovskite film, leading to relaxed microstrain and a lower defect concentration. As a result, a PCE of 25.4% for rigid PSCs and a record PCE of 23.6% (certified 22.5%) for FPSCs have been achieved. In addition, the corresponding FPSCs exhibited excellent bending durability, maintaining ~85% of their initial efficiency after bending at a 6 mm radius for 10 000 cycles.

INTRODUCTION

Perovskite solar cells (PSCs) have emerged as a cost-effective photovoltaic technology, as is obvious from the power-conversion efficiency (PCE), which has surpassed 25.7%.^{1–4} With a high power-to-weight ratio and excellent flexibility, flexible PSCs (FPSCs) hold promise as power sources for flexible electronic devices, wearable equipment, and spacecraft.⁵ With the experience accumulated in rigid PSCs, the PCE of FPSCs has reached over 22% in small areas^{6,7} and 15% in large areas.^{8,9} In addition, an increasing number of researchers have begun to explore the industrial roll-to-roll fabrication of FPSCs,^{10,11} showing a promising future in flexible photovoltaic applications.

However, the PCE of FPSCs still lags far behind that of rigid PSCs, which can be mainly attributed to the inferior perovskite thin film quality on flexible substrates compared with that of glass substrates. The difference in the physical properties of glass substrates and flexible plastic substrates, such as thermal properties and surface roughness, increases the difficulty in obtaining high-quality perovskite thin films on plastic substrates.¹² Additives comprising small molecules and polymers were employed in the perovskite precursor to regulate the perovskite crystallization process,¹³ improve crystallization, strengthen the perovskite crystals,¹⁴ and passivate defects.¹⁵

Due to their polycrystalline nature, perovskite films also suffer from the influence of strain on the optoelectronic properties and stability.^{16,17} The residual strain is related to the stability of the perovskite¹⁸ and usually

accelerates its degradation by increasing ion migration and reducing perovskite structural stability.¹⁹ The microstrain, which originates from local lattice mismatch or misorientation and is related to the local lattice disorder and defects,²⁰ is highly detrimental to the perovskite film and thus urgently needs to be mitigated. Although modifying the perovskite lattice by cation doping, such as Cd²⁺²¹ and MDA²⁺,²² has been demonstrated to lower microstrain for efficient and stable PSCs, the strain related to environmental effects such as bending, which is extremely important for FPSCs, cannot be alleviated by the above-mentioned method.

In this work, we judiciously designed a novel multifunctional additive, methylammonium succinate (MS), to alleviate strain and passivate interface defects in a perovskite film. It has been reported that FAI-terminated surfaces and Pbl₂-terminated surfaces are stable surfaces in FAPbI₃ grains.²³ The two terminal carboxyl groups in MS can form hydrogen bonds with formamidinium (FA) with two neighboring perovskite grains, while the ethylene group between the two carboxyl groups provides flexibility to release the strain caused by environmental effects such as thermal stress and bending of flexible devices, leading to perovskite films with reduced defects and enhanced durability. In addition, the carboxyl group can coordinate with the dangling Pb²⁺ present at the surface of perovskite grains, and the MA⁺ can compensate for the A position vacancy in the ABX₃ perovskite, reducing the number of defects. As a result, we achieved a high PCE of 25.4% and 23.6% (certified 22.5%) for rigid and flexible PSCs, respectively, which is the highest reported PCE for FPSCs (Figure 1A) to date. In addition, the bilateral anions bind strongly with the perovskite grain surfaces, strengthening the grain boundaries (Figure 1B) and releasing the strain during the bending process. Therefore, the FPSCs exhibited improved bending durability, retaining ~85% of their initial efficiency after 10 000 bending cycles (at a 6 mm radius).

RESULTS AND DISCUSSION

The grain boundaries of perovskite thin films are rich in defects and the start points of the cracks, corrosion, and decomposition. The multifunctional additive MS was designed to heal the defects and strengthen the grain boundaries by interacting with two adjacent grain boundaries.

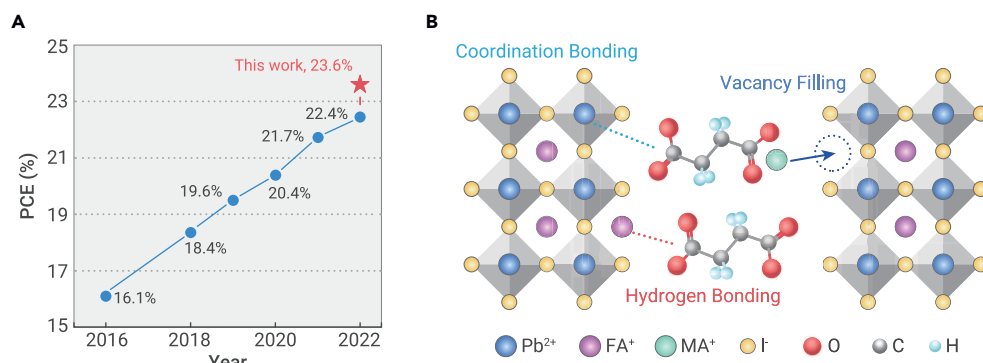


Figure 1. PCE result and the functions of the MS additive (A) Summarized PCE development of FPSCs with this work highlighted. **(B)** Proposed mechanism of the bilateral MS molecule at the perovskite grain boundaries.

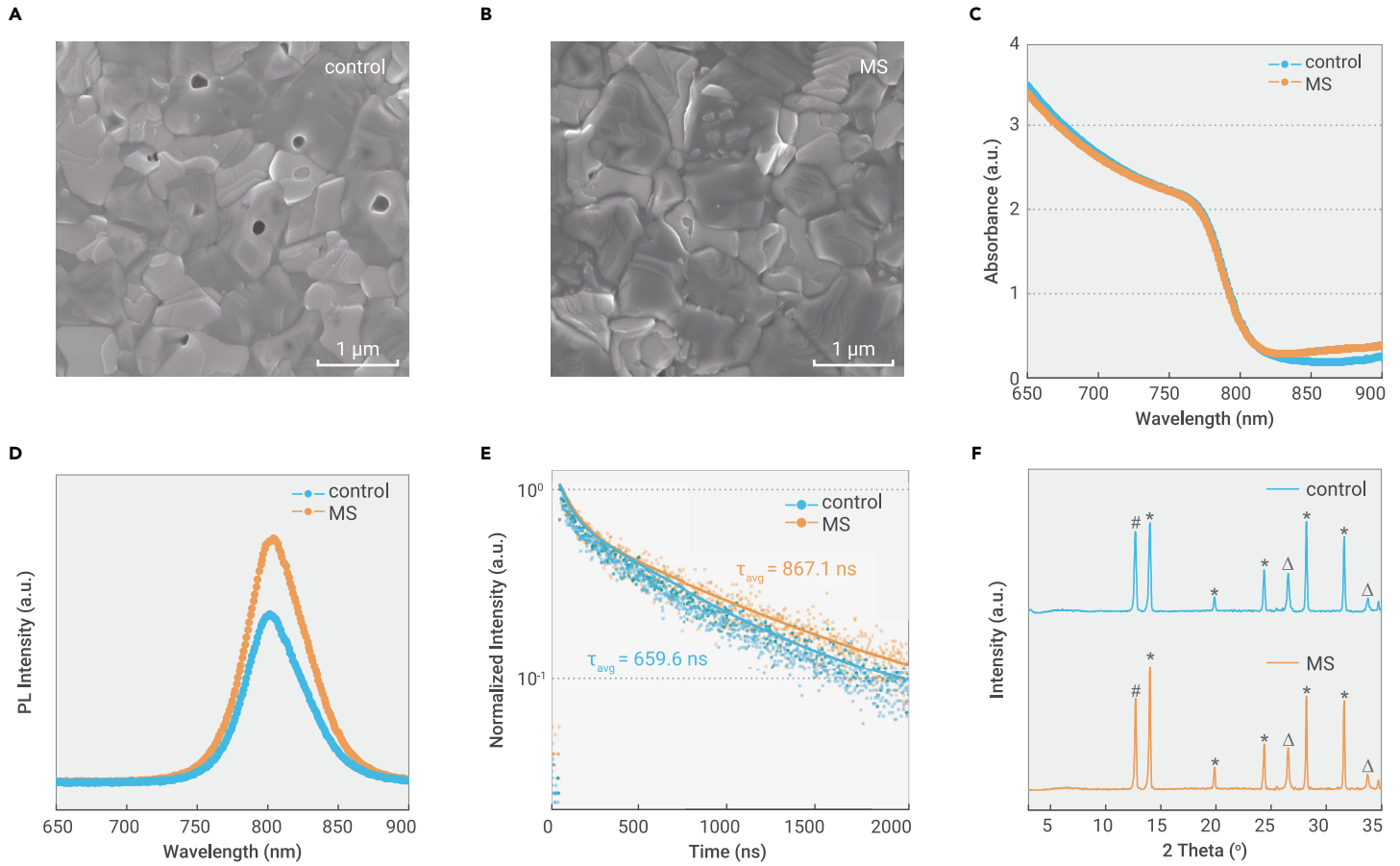


Figure 2. Perovskite thin film characterization (A–F) Scanning electron microscopy (SEM) images of top-view morphology (**A and B**), UV–visible spectra (**C**), static photoluminescence spectra (**D**), time-resolved photoluminescence decay (**E**), and X-ray diffraction pattern (**F**) of the control and MS-perovskite films (# denotes the PbI_2 phase, * denotes the FAPbI_3 perovskite phase, and Δ denotes the FTO substrate).

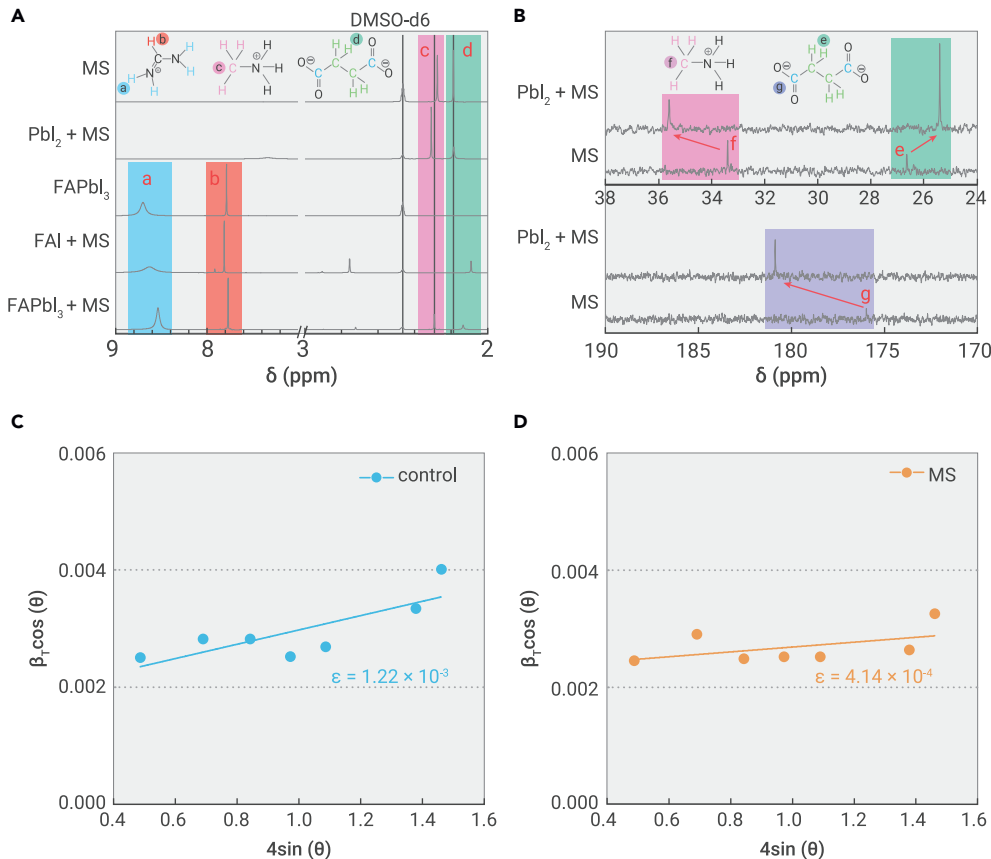


Figure 3. Interaction between the MS molecule and FAPbI_3 perovskite (A) ^1H -NMR result reveals that MS interacts with Pb^{2+} ions (MA^+ cations) and FA^+ ions (succinate $^{2-}$ anions). **(B)** ^{13}C -NMR result reveals that $-\text{COO}^-$ groups interact with PbI_2 . **(C and D)** Microstrains in control and MS-perovskite thin films.

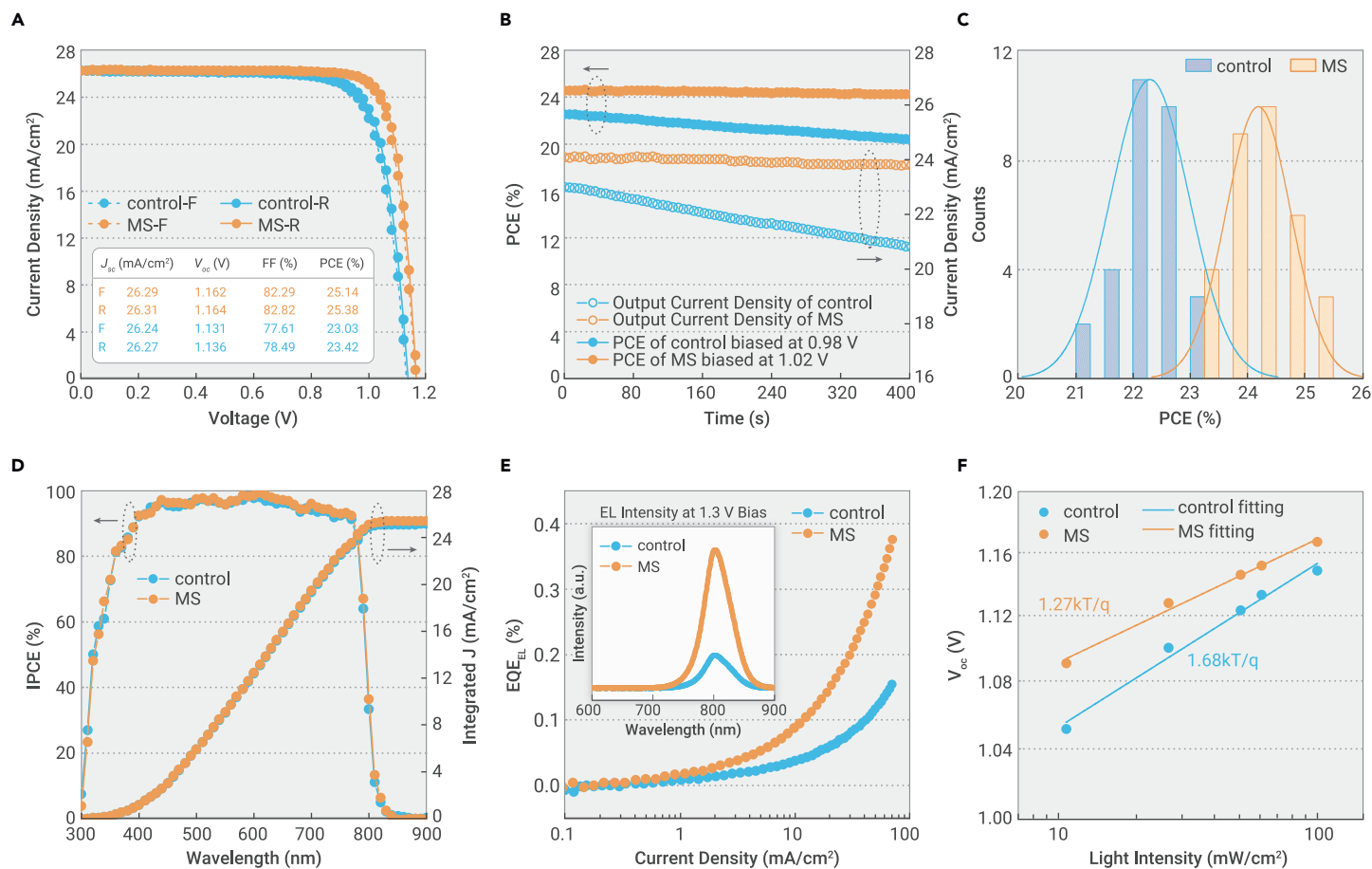


Figure 4. Photovoltaic characterization of the PSCs on glass substrates (A) J - V curves and photovoltaic metrics of the champion control and MS-PSCs. **(B)** Stable power output of the champion control and MS-PSCs at 0.98 and 1.02 V, respectively. **(C)** PCE distribution of control and MS-PSCs. **(D)** IPCE and the integrated J_{sc} curves of the control and MS-PSCs. **(E)** EQE_{EL} at different current densities and EL spectra of the control and MS-PSCs. **(F)** V_{oc} versus light intensity and linear fit for the control and MS-PSCs.

With two terminal carboxyl groups, the succinate can bond with FA^+ cations via hydrogen bonds and coordinate with dangling Pb^{2+} in the grain boundaries. To investigate the effect of the MS additives, FAPbI₃ perovskite thin films were fabricated by a conventional sequential deposition method as previously reported.^{24,25} The acquired perovskite thin films are denoted "control" and "MS-perovskite" for the films without and with MS additive (in PbI_2 solution), respectively. The surface scanning electron microscopy images of the control and MS-perovskite film morphologies are shown in Figures 2A and 2B. A small amount (~0.4 mol %) of MS additive resulted in a smoother surface, and the holes sighted in the control film were diminished. The cross-sectional images (Supplemental Figure 1) show that more grain boundaries exist near the control perovskite/ SnO_2 interface, while the MS-perovskite film looks more uniform.

Detailed studies of the photophysical properties of the films indicate that MS incorporation improves the perovskite film quality without sacrificing light absorption. The absorption spectra (Figure 2C) and extracted band gap from the Tauc plot (Supplemental Figure 2) are almost identical for both films. This means that the MS additive did not compromise the light absorbing and absorption edge of the FAPbI₃ perovskite thin film. Photoluminescence (PL) spectra did not show any obvious peak shift either (Figure 2D). However, the MS-perovskite sample demonstrates a stronger PL intensity and longer PL lifetime (τ_{avg} = 867.1 versus 659.6 ns for the control sample; Figure 2E), revealing a reduced defect concentration in the perovskite film after MS incorporation. These results indicate that the MS molecule contributed to an improved thin film quality of the FAPbI₃ perovskite films.

Figure 2F shows the X-ray diffraction (XRD) patterns of the control and MS-modified films on the FTO substrates. It should be noted that residual PbI_2 is common in two-step-processed perovskite films.^{26,27} On the other hand, the XRD patterns show no detectable peak shift

or new peak arising in the MS-modified film. Therefore, we speculate that the MS molecule should not be incorporated into the FAPbI₃ lattice but is mainly located in the grain boundaries. The bilateral structure of the MS molecule enables it to bond from both sides. Nuclear magnetic resonance (NMR) measurements were performed to elucidate the interaction mechanism between the MS molecule and the FAPbI₃ perovskite. As illustrated in the ¹H-NMR spectra (Figure 3A), for the two parts of the MS molecule, the MA^+ cation tends to interact with the inorganic PbI_2 , as indicated by the shift of $-CH_3$ groups at approximately 2.3 ppm after mixing PbI_2 in the precursor solution. On the other hand, the succinate²⁻ anion prefers to bond with the FA^+ cation via $N-H \cdots O$ hydrogen bonding, as indicated by the prominent shift of the resonance peak of the $-NH_2$ groups in FA^+ . The shift of the COO^- group in the ¹³C-NMR spectra (Figure 3B) indicates the interaction between Pb^{2+} and succinate²⁻ anions. In a word, the NMR results indicate that succinate²⁻ can bond with both FA^+ and Pb^{2+} . To compare the strength of the interactions, we calculated the absorption energy of succinate anions on the two kinds of perovskite surfaces (FAI terminated and PbI_2 terminated) by density functional theory. Negative absorption energy values are obtained in both situations, -4.86 eV in the FAI-terminated state and -4.16 eV in the PbI_2 -terminated situation, which indicates a stronger interaction between the succinate anion and FA^+ cations. We speculated that MS interacts more with FA^+ -related defects by forming hydrogen bonds with FA cations, suppressing the formation of FA vacancies.

To evaluate the effects of MS additives on the perovskite crystal structure, we first performed grazing incidence XRD characterizations to analyze the residual strain of the perovskite films.^{28,29} Both control and MS-perovskite were almost strain free, while MS-perovskite showed a slightly compressed manner (Supplemental Figure 3). We consider this reasonable

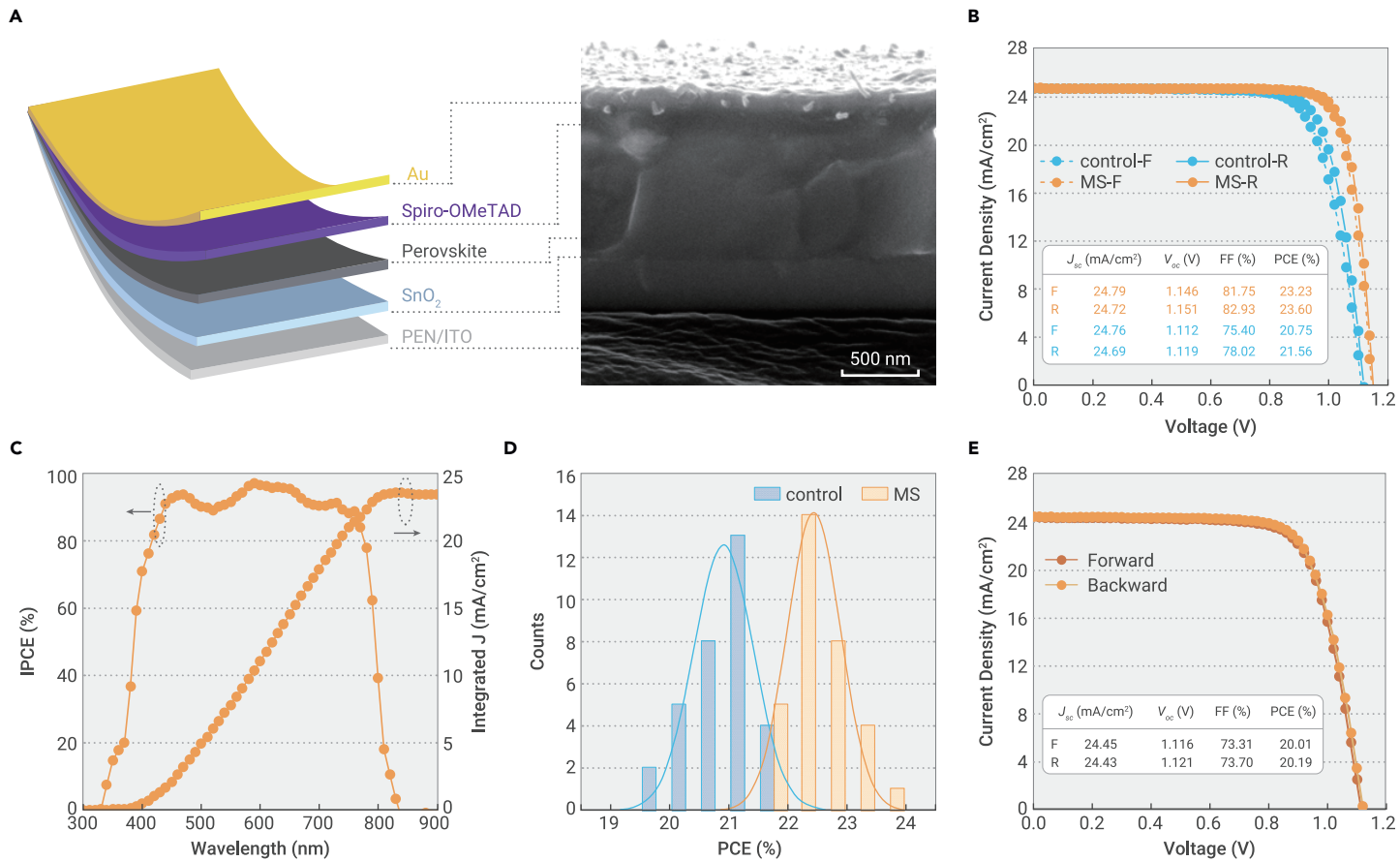


Figure 5. Photovoltaic characterization of the FPSCs (A) Device structure and the cross-sectional SEM image of the MS-FPSC. **(B)** J - V curves and photovoltaic metrics of the champion FPSCs. **(C)** IPCE and the integrated J_{sc} of the champion MS-FPSC. **(D)** Statistical distribution of the PCE of control and MS-FPSCs. **(E)** J - V curve of the 1 cm² aperture area MS-FPSC.

because residual strain is affected by the thermal expansion mismatch between perovskite and substrates,³⁰ while the perovskite composition, substrates, and annealing process were all the same in our case. We further analyzed the microstrain in the perovskite films through the Williamson-Hall equation:³¹

$$\beta_T \cos \theta = \epsilon (4 \sin \theta) + \frac{K\lambda}{D},$$

where β_T is the full width at half maximum of the perovskite peaks in the XRD patterns, θ is the diffraction angle, K is the shape factor, λ is the wavelength of the X-ray source, and D is the crystallite size. The equation represents a linear relationship between $\beta_T \cos \theta$ and $4 \sin \theta$, and the slope ϵ extracted here reveals the microstrain in the films. The MS additive effectively reduced the microstrain in the FAPbI₃ thin films from 1.22×10^{-3} to 4.14×10^{-4} (Figures 3C and 3D). As indicated by NMR measurements, the succinate anions can bond with FA⁺ and Pb²⁺ atoms, which in turn can potentially suppress lattice defects and distortion at the grain boundaries, which will be beneficial to alleviate the microstrain in the perovskite films.²⁰ To exclude the crystalline size effect on the peak broadening of XRD patterns, we estimated the averaged crystalline sizes through the Scherrer equation:²²

$$D = \frac{K\lambda}{\beta \cos \theta}$$

The averaged crystalline sizes barely changed from 55.2 to 56.3 nm (Supplemental Table 5). Therefore, we concluded that the peak-broadening difference here mainly comes from the microstrain and that the crystal size effect contributes little. Previous reports have found that such microstrain in perovskite films is unfavorable for both PSC efficiency and stability.^{21,22} The reduced microstrain is

in line with the reduced defect concentration revealed by PL characterization,²² which will be beneficial for the performance enhancement of PSCs. We also performed strain analysis for the flexible devices. The residual strain of the perovskite films on flexible substrates is higher than that of rigid substrates, which might be related to the different film growth process, arising from the roughness difference of flexible and rigid substrates.⁸ Compared with the pristine perovskite film, a slightly lower residual tensile strain is obtained in the MS-perovskite (Supplemental Figure 4), which is favorable for the FPSCs. As shown in Supplemental Figure 5, the XRD patterns show strong features of PEN substrates. Nevertheless, we can elucidate the microstrains by analyzing the perovskite peaks not overlapped with PEN with Williamson-Hall equation, showing a reduced microstrain for the MS-perovskite film (Supplemental Figure 6), which is favorable for the performances of the FPSCs.

The performances of the PSCs without and with MS incorporation were investigated by J - V characterization. Devices were fabricated based on the standard configuration using SnO₂ and spiro-OMeTAD as electron- and hole-transporting layers, respectively. The J - V curves of the champion control and MS-PSCs are shown in Figure 4A. The control device demonstrated a PCE of 23.4%. The MS-PSC reached a higher efficiency of 25.4%, with a short-circuit current density (J_{sc}) of 26.31 mA/cm², an open-circuit voltage (V_{oc}) of 1.164 V, and fill factor of 82.82%. The unencapsulated MS-PSC showed a stable power output at 1.02 V bias with a PCE of ~24.5% during the recorded 400 s in air (Figure 4B), reflecting the excellent short-term stability, while the control device dropped obviously from 22.5% to ~20.5%. Moreover, the statistical distribution confirmed the overall improvement brought by MS incorporation, especially in the PCE (Figure 4C) and V_{oc} (Supplemental Figure 7).

The incident photon-to-current conversion efficiency (IPCE) results shown in Figure 4D verified the measured J_{sc} . The IPCE spectra of the control and modified devices show only small differences. The integrated J_{sc} of the control and MS-PSCs are 25.15 and 25.54 mA/cm², respectively, which matches well with the

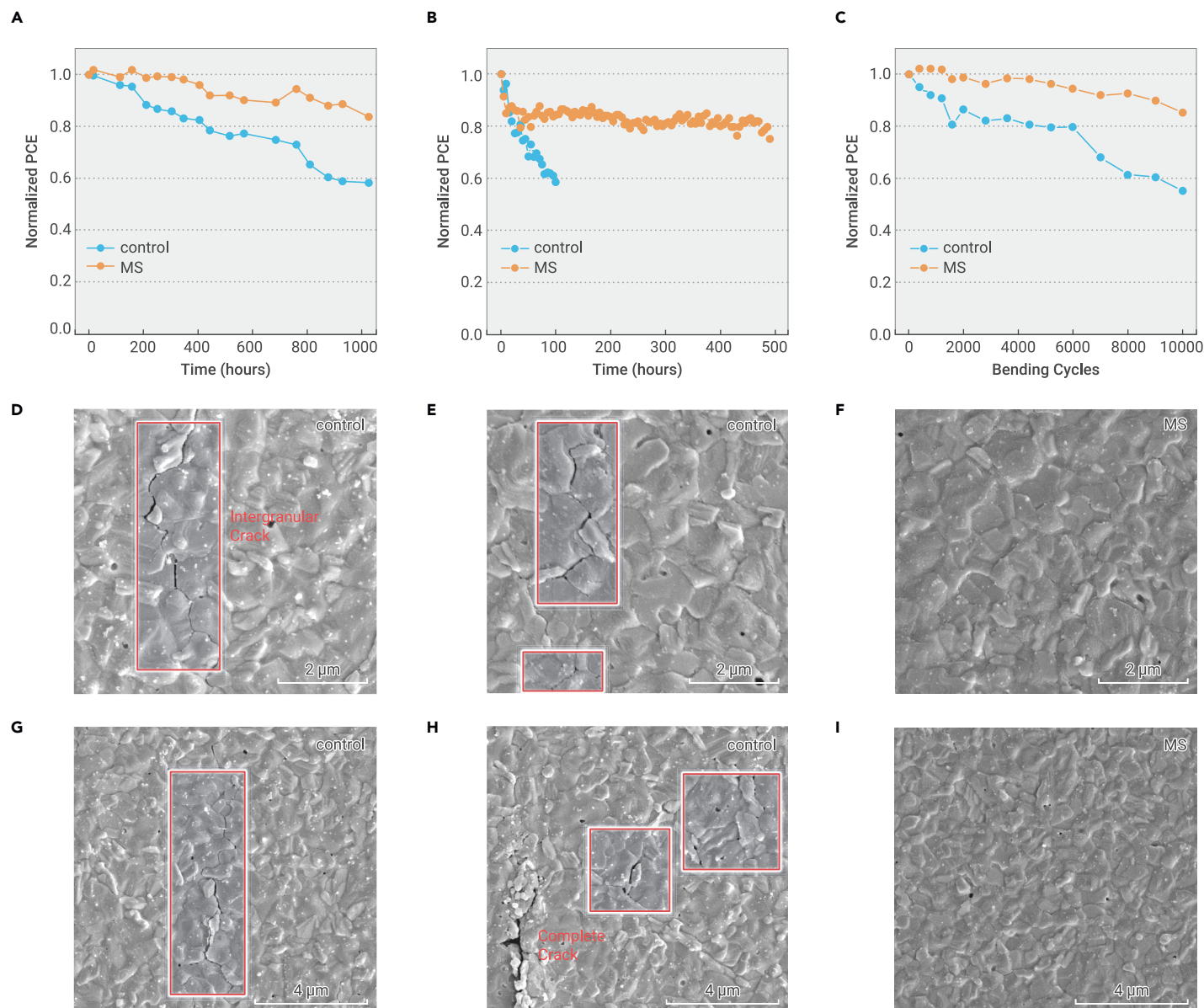


Figure 6. Tracked stability of the solar cell devices (A) The stability of the unencapsulated control and MS-PSCs under $\sim 30\%$ relative humidity. (B) Long-term stability of the unencapsulated PSCs under continuous light irradiation in a N_2 atmosphere. (C) The bending stability of FPSCs ($R = 6$ mm, $\sim 30\%$ relative humidity, $\sim 25^\circ C$). (D–I) Top-view SEM images of the perovskite film from FPSCs after 10 000 bending cycles at 6 mm, with the Au electrode removed by tape and spiro-OMeTAD removed by chlorobenzene.

J-V analysis. Electroluminescence (EL) was conducted to reveal the nonradiative recombination in the PSCs (Figure 4E). The MS device not only shows a more pronounced electroluminescence intensity at 1.3 V but also demonstrates a higher external quantum efficiency (EQE) for all applied currents, indicating suppressed nonradiative recombination in the perovskite. The relationship between V_{oc} and the light intensity is investigated to determine the ideality factor n , which is related to trap-assisted recombination. The lower n (1.27) of the MS device than that of the control device (1.68) indicates the reduced trap-assisted recombination of the MS device (Figure 4F). Moreover, transient photovoltage decay (Supplemental Figure 8A) and space-charge-limited current measurements (Supplemental Figure 9) further support the reduced trap densities and improved V_{oc} and device performance.

The bilateral structure of the MS molecule, which is able to bind strongly with grain boundaries and relax microstrain, should be beneficial for the mechanical durability of perovskite films. This inspired us to fabricate MS-perovskite-based FPSC devices using PEN/ITO substrates (Figure 5A). Figure 5B demonstrates the *J-V* curves and photovoltaic metrics for the champion FPSC with and without MS incorporation. The champion MS-FPSC had a maximum PCE of 23.6% in the reserve scan, along with a

J_{sc} of 24.72 mA cm^{-2} , a V_{oc} of 1.151 V, and a fill factor of 82.93%, exceeding the 21.6% PCE of champion control. This outstands as the highest PCE reported for FPSCs.^{6,7,9,32,33} The champion device showed little hysteresis, which reached 23.2% in the forward scan. The integrated J_{sc} deduced from the IPCE measurement also reached 23.44 mA cm^{-2} (Figure 5C), which is consistent with that acquired from *J-V* analysis. To further verify the measured efficiency, we sent one of our MS-FPSCs for certification, which displays a certified efficiency of 22.5% with a stabilized power output efficiency of $\sim 22.0\%$ at 1.01 V bias (Supplemental Figure 13). The quasi-steady-state and stabilized efficiency both rank as the highest in all certified FPSCs.^{6,7} The overall improvement of the FPSC performance is outstanding (Figure 5D), in line with the results obtained on rigid PSCs. The application of the MS additive also demonstrated over 20% PCE for the large-area 1 cm^2 device (Figure 5E), which could be higher with further optimization.⁴

The stability of the PSCs was measured, and the MS-PSCs demonstrated improved resistance to humidity and operation conditions. We first tracked the shelf-life stability of the unencapsulated PSCs. After 1000 h of storage under $\sim 30\%$ relative humidity, the control device

lost ~40% of the initial PCE, while the MS device showed a slower degradation of ~15% (Figure 6A). The enhanced humidity resistance can be attributed to the hydrophobic alkyl chain located at the grain boundaries, which is the main channel for water infiltration. Unencapsulated devices were also aged under continuous light soaking in our homemade maximum power point tracking system at 25°C in a N₂ atmosphere to further assess the long-term operational stability (Figure 6B). Despite experiencing a rapid burn in, the power output of the MS-PSC maintained >80% of the initial PCE for ~500 h. However, the PCE of the control device dropped quickly to ~60% of its initial value after 100 h, in good agreement with the short-term stability displayed in Figure 4B. It is well known that the degradation process in perovskite starts mainly from the grain boundaries.³⁴ As revealed by the PL and NMR measurements, the MS additive not only reduced the defects in the bulk perovskite but also strengthened the perovskite lattice structure via hydrogen bonding at the grain boundaries, which contributed to the enhanced operational stability.^{35,36}

For mechanical stability, we performed a continuous bending test to evaluate the mechanical durability of FPSC devices and recorded their efficiency change during the test. The control FPSC gradually dropped to 60% of the initial PCE after 10 000 bending cycles (bending radius 6 mm), while the MS-FPSC retained ~85% of its initial PCE (Figure 6C), indicating improved mechanical durability of the modified devices. The improved mechanical stability of the MS-FPSC could be attributed to the strengthened grain boundaries and relaxed microstrain, which inhibited perovskite fracture and defect formation.^{21,37} We further observed the morphology change of the perovskite film of the devices after the cyclic bending test. The metal electrode and the spiro-OMeTAD layer were removed to expose the perovskite layer. The crack in the control film is obvious and mainly develops inter granularly (Figures 6D and 6E). In contrast, the MS-perovskite film shows no cracks (Figures 6F and 6I). The well-maintained film morphology could also inhibit moisture infiltration in the ambient environment in our bending,³² which further confirmed the improved stability of the MS-FPSCs. In addition, we performed a bending test with a radius of 5 mm. Although both devices degraded faster than that of the 6 mm bending test, possibly due to ITO fracture, the MS-FPSC showed a T80 4 times longer than that of the control FPSC (Supplemental Figure 15).

CONCLUSION

In conclusion, we demonstrated the incorporation of bilateral MS molecules into a perovskite thin film for high performance and stable PSCs. The additive molecule effectively reduces the microstrain in the FAPbI₃ perovskite thin film, resulting in improved quality and reduced defect concentration of the thin film. High-efficiency PSCs were fabricated on both rigid substrates and flexible PEN substrates. Specifically, FPSCs with MS incorporation showed an impressively high efficiency of 23.6% (certified 22.5%), which ranks as the highest value in the reported literature to date. Furthermore, MS-FPSCs showed improved bending durability, retaining ~85% of the initial efficiency after 10 000 bending cycles. The efficiency and mechanical stability of the FPSCs are closely related to the microstrain of the perovskite film. This work provides a new solution to reduce microstrain by using a multifunctional organic additive that does not incorporate into the perovskite lattice but strengthens the grain boundaries and heals the defects. A variety of new molecules with similar supermolecular interactions such as hydrogen bond, coordination, and halogen bond can be designed to alleviate microstrain, which will further improve the performances and stability of FPSCs, promoting the large-scale application of this power sources.

METHODS

Please refer to the supplemental information for details on methods.

REFERENCES

- NREL best research-cell efficiency chart. <https://www.nrel.gov/pv/assets/pdfs/best-research-cell-efficiencies-rev220126.pdf>.
- Zhang, F., Park, S.Y., Yao, C., et al. (2022). Metastable Dion-Jacobson 2D structure enables efficient and stable perovskite solar cells. *Science* **375**, 71–76.
- Li, X., Zhang, W., Guo, X., et al. (2022). Constructing heterojunctions by surface sulfidation for efficient inverted perovskite solar cells. *Science* **375**, 434–437.
- Wang, S., Tan, L., Zhou, J., et al. (2022). Over 24% efficient MA-free Cs_xFA_{1-x}PbX₃ perovskite solar cells. *Joule* **6**, 1344–1356.
- Hu, Y., Niu, T., Liu, Y., et al. (2021). Flexible perovskite solar cells with high power-per-weight: progress, application, and perspectives. *ACS Energy Lett.* **6**, 2917–2943.
- Zheng, Z., Li, F., Gong, J., et al. (2022). Pre-buried additive for cross-layer modification in flexible perovskite solar cells with efficiency exceeding 22. *Adv. Mater.* **34**, 2109879.
- Yang, L., Feng, J., Liu, Z., et al. (2022). Record-efficiency flexible perovskite solar cells enabled by multifunctional organic ions interface passivation. *Adv. Mater.* **34**, 2201681.
- Dai, X., Deng, Y., Van Brackle, C.H., et al. (2019). Scalable fabrication of efficient perovskite solar modules on flexible glass substrates. *Adv. Energy Mater.* **10**, 1903108.
- Chung, J., Shin, S.S., Hwang, K., et al. (2020). Record-efficiency flexible perovskite solar cell and module enabled by a porous-planar structure as an electron transport layer. *Energy Environ. Sci.* **13**, 4854–4861.
- Othman, M., Zheng, F., Seeber, A., et al. (2022). Millimeter-sized clusters of triple cation perovskite enables highly efficient and reproducible roll-to-roll fabricated inverted perovskite solar cells. *Adv. Funct. Mater.* **32**, 2110700.
- Li, H., Zuo, C., Angmo, D., et al. (2022). Fully roll-to-roll processed efficient perovskite solar cells via precise control on the morphology of PbI₂:CsI layer. *Nano-Micro Lett.* **14**, 79.
- Jung, H.S., Han, G.S., Park, N.-G., and Ko, M.J. (2019). Flexible perovskite solar cells. *Joule* **3**, 1850–1880.
- Feng, J., Zhu, X., Yang, Z., et al. (2018). Record efficiency stable flexible perovskite solar cell using effective additive assistant strategy. *Adv. Mater.* **30**, e1801418.
- Hu, X., Huang, Z., Li, F., et al. (2019). Nacre-inspired crystallization and elastic “brick-and-mortar” structure for a wearable perovskite solar module. *Energy Environ. Sci.* **12**, 979–987.
- Yang, L., Xiong, Q., Li, Y., et al. (2021). Artemisinin-passivated mixed-cation perovskite films for durable flexible perovskite solar cells with over 21% efficiency. *J. Mater. Chem.* **9**, 1574–1582.
- Liu, D., Luo, D., Iqbal, A.N., et al. (2021). Strain analysis and engineering in halide perovskite photovoltaics. *Nat. Mater.* **20**, 1337–1346.
- Cheng, Y., and Ding, L. (2021). Pushing commercialization of perovskite solar cells by improving their intrinsic stability. *Energy Environ. Sci.* **14**, 3233–3255.
- Rolston, N., Bush, K.A., Printz, A.D., et al. (2018). Engineering stress in perovskite solar cells to improve stability. *Adv. Energy Mater.* **8**, 1802139.
- Zhao, J., Deng, Y., Wei, H., et al. (2017). Strained hybrid perovskite thin films and their impact on the intrinsic stability of perovskite solar cells. *Sci. Adv.* **3**, eaao5616.
- Wu, J., Liu, S.-C., Li, Z., et al. (2021). Strain in perovskite solar cells: origins, impacts and regulation. *Natl. Sci. Rev.* **8**, nwab047.
- Saidaminov, M.I., Kim, J., Jain, A., et al. (2018). Suppression of atomic vacancies via incorporation of isovalent small ions to increase the stability of halide perovskite solar cells in ambient air. *Nat. Energy* **3**, 648–654.
- Kim, G., Min, H., Lee, K.S., et al. (2020). Impact of strain relaxation on performance of α -formamidinium lead iodide perovskite solar cells. *Science* **370**, 108–112.
- Oner, S.M., Sezen, E., Yordanli, M.S., et al. (2022). Surface defect formation and passivation in formamidinium lead triiodide (FAPbI₃) perovskite solar cell absorbers. *J. Phys. Chem. Lett.* **13**, 324–330.
- Zhou, J., Li, M., Wang, S., et al. (2022). 2-CF₃-PEAI to eliminate Pb⁰ traps and form a 2D perovskite layer to enhance the performance and stability of perovskite solar cells. *Nano Energy* **95**, 107036.
- Li, M., Zhou, J., Tan, L., et al. (2022). Brominated PEAi as multi-functional passivator for high-efficiency perovskite solar cell. *Energy Environ. Mater.* **5**, eem2.12360.
- Yang, X., Fu, Y., Su, R., et al. (2020). Superior carrier lifetimes exceeding 6 μ s in polycrystalline halide perovskites. *Adv. Mater.* **32**, 2002585.
- Xue, J., Wang, R., Chen, X., et al. (2021). Reconfiguring the band-edge states of photovoltaic perovskites by conjugated organic cations. *Science* **371**, 636–640.
- Zhu, C., Niu, X., Fu, Y., et al. (2019). Strain engineering in perovskite solar cells and its impacts on carrier dynamics. *Nat. Commun.* **10**, 815.
- Li, F., Deng, X., Qi, F., et al. (2020). Regulating surface termination for efficient inverted perovskite solar cells with greater than 23% efficiency. *J. Am. Chem. Soc.* **142**, 20134–20142.
- Xue, D.-J., Hou, Y., Liu, S.-C., et al. (2020). Regulating strain in perovskite thin films through charge-transport layers. *Nat. Commun.* **11**, 1514.
- Williamson, G.K., and Hall, W.H. (1953). X-ray line broadening from filed aluminium and wolfram. *Acta Metall.* **1**, 22–31.
- Dong, Q., Chen, M., Liu, Y., et al. (2021). Flexible perovskite solar cells with simultaneously improved efficiency, operational stability, and mechanical reliability. *Joule* **5**, 1587–1601.
- Wu, S., Li, Z., Zhang, J., et al. (2021). Low-bandgap organic bulk-heterojunction enabled efficient and flexible perovskite solar cells. *Adv. Mater.* **33**, 2105539.
- Jeong, J., Kim, M., Seo, J., et al. (2021). Pseudo-halide anion engineering for α -FAPbI₃ perovskite solar cells. *Nature* **592**, 381–385.
- Li, X., Dar, M.I., Yi, C., et al. (2015). Improved performance and stability of perovskite solar cells by crystal crosslinking with alkylphosphonic acid omega-ammonium chlorides. *Nat. Chem.* **7**, 703–711.
- Bai, S., Da, P., Li, C., et al. (2019). Planar perovskite solar cells with long-term stability using ionic liquid additives. *Nature* **571**, 245–250.
- Huang, Z., Hu, X., Liu, C., et al. (2017). Nucleation and crystallization control via polyurethane to enhance the bendability of perovskite solar cells with excellent device performance. *Adv. Funct. Mater.* **27**, 1703061.

ACKNOWLEDGMENTS

This work was supported by the National Natural Science Foundation of China (no. 21872080) and projects supported by the State Key Laboratory of Power System and

Generation Equipment (nos. SKLD21Z03 and SKLD20M03), the Chinese Thousand Talents Program for Young Professionals, and State Grid Corporation of China, National Bio Energy Co., Ltd. This work was also supported by grant no. 52789922000D, China Huaneng Group Co., Ltd., and grant no. HNKJ20-H88.

AUTHOR CONTRIBUTIONS

C.Y. conceived the idea and directed the project. M.L., J.Z., and L.T. performed the experiments. M.L. prepared the draft. All the authors participated in the discussion of the results and revision of the manuscript. The lead contact's websites are as follows: <https://www.x-mol.com/groups/Tsinghua-EEA-312lab?lang=en> and <https://www.eea.tsinghua.edu.cn/en/faculties/yicy.htm>.

DECLARATION OF INTERESTS

The authors declare no competing interests.

SUPPLEMENTAL INFORMATION

Supplemental information can be found online at <https://doi.org/10.1016/j.xinn.2022.100310>.

LEAD CONTACT WEBSITE

<https://www.x-mol.com/groups/Tsinghua-EEA-312lab?lang=en>.

<https://www.eea.tsinghua.edu.cn/en/faculties/yicy.htm>.